BULLETIN OF THE EARTHQUAKE
RESEARCH INSTITUTE
UNIVERSITY OF TOKYO
Vol. 69 (1994) pp. 1–18

Aftershock Distribution of the 1993 M6.6 Earthquake Off Noto Peninsula and its Relation to Tectonic Features

Tameshige TSUKUDA,[1] Hiroo WADA,[2] Kaname SAKAI[1] and Kiyoshi ITO[2]

[1]Earthquake Research Institute, University of Tokyo
[2]Disaster Prevention Research Institute, Kyoto University

(Received December 28, 1993)

Abstract

An M6.6 earthquake occurred on February 7, 1993, around a sea rise extending southwest-northeast direction off the northeastern tip of Noto Peninsula. The hypocenters of the mainshock and aftershocks were located using telemetered data from university stations. The aftershocks during the first two days are concentrated in the narrow active fault zone along the northwest side of the rise. Other concentrations occurred along active faults on the southeast side of the rise. Most of the focal depths are 10–15km, consistent with the interpretation of T phases and pP phases recorded at some stations.

Northwestward dipping 3-dimensional distributions for large aftershocks suggest two possible fault planes, which coincide well with the two fault planes of the CMT solution. The gross nature of the seismic fault is of a thrust type, which contradicts the strike slip solution estimated from the initial motions.

The Noto region is part of the tectonic zone along the eastern margin of the Japan Sea, where zonal shortening due to compression is predominant as in the Japan Sea coast region in northern Honshu, Japan. The alignment of aftershocks along the topographic lineaments and submarine active faults may reflect this tectonism.

Introduction

The northeastern tip of Noto Peninsula was struck by one of the biggest earthquakes in history on February 7, 1993 at 22:27 JST. The epicentral area is shown in Figs. 1 and 2. The magnitude 6.6 of this earthquake is comparable to that of the August 1, 1729 event in northern Noto Peninsula, the biggest historical earthquake on the peninsula. The damage was mostly restricted to Suzu City, which occupies the northern tip of Noto Peninsula. According to newspapers and a quick report of the field survey of damage edited by KITAURA (1993), principal damage to buildings, structures, life lines and human beings was as follows:

(1) Damage to buildings was concentrated in the center of Suzu City (see Fig. 2), northeastern Noto Peninsula. In this city, 6 residential houses were destroyed, one completely, and several storehouses were collapsed. Diatomaceous clay from collapsing hillside crushed the inner and front buildings of a Shinto shrine in the city.

(2) Collapse of a road tunnel roof in Orito, Suzu City, at the northern end of Noto Peninsula stopped traffic. A passenger car on a city road in Suzu City fell into a cave-in caused by

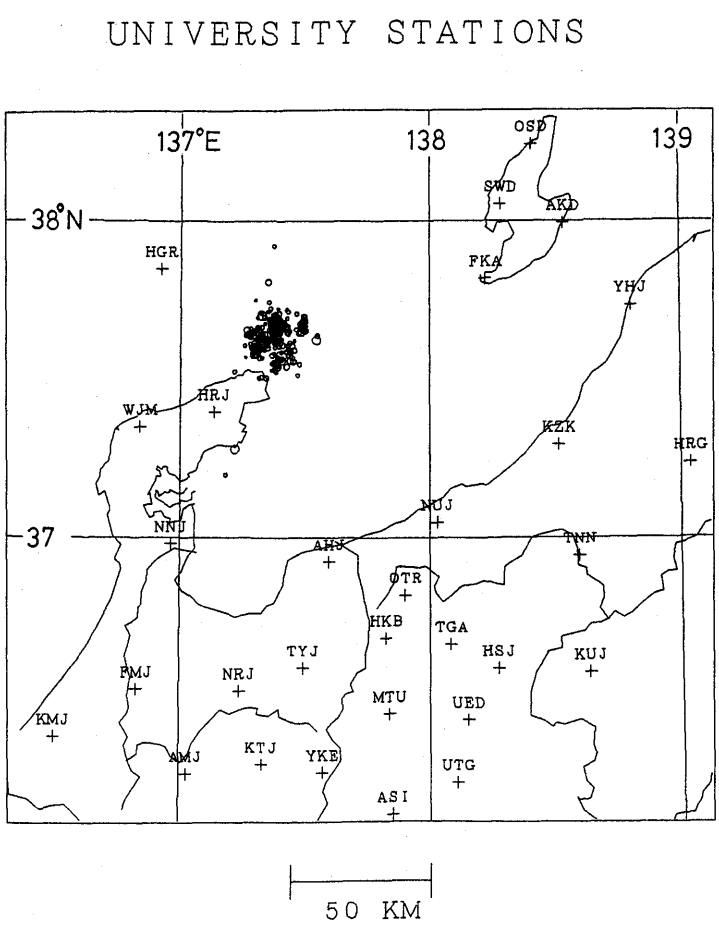

Fig. 1. Location of the source area of the 1993 off Noto Peninsula earthquake and distribution of university seismic stations. Aftershock distribution is the same as in Fig. 2.

the earthquake; fortunately the driver was saved with slight injury.

(3) In Suzu City 1100 houses suffered from suspension of water supply for one day. A fire broke out in Kanazawa City more than 130km southwest from the source area. Astonishingly, no other fires were reported although it was winter when many people would use gas or oil heaters.

(4) The number of wounded persons were 29 in Suzu City; one was seriously injured. Among them 6 persons suffered from heat when they tried to stop stoves; some were exposed to hot water. Others were bruised or scratched by falling pieces of furniture, ceilings and doors or by falling down steps. No fatalities were reported.

The purpose of this paper is to present precise distributions of aftershock hypocenters in reference to that of the mainshock derived by data from recently established high sensitivity seismic observation networks and to make clear the relation to the tectonic

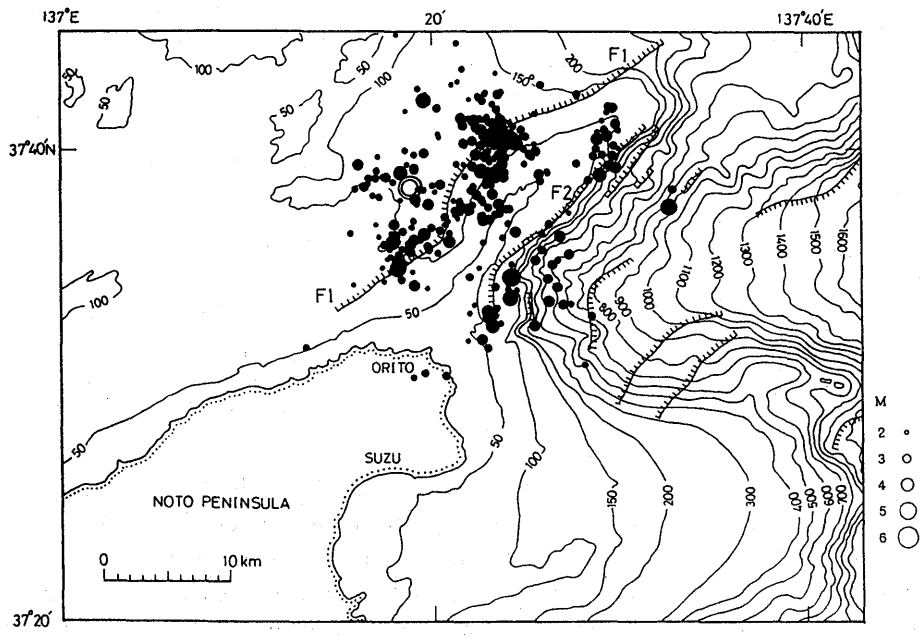

Fig. 2. Epicentral distribution of aftershocks, and the topographic map around the source region. The mainshock is represented by a double circle. The bathymetric height contours are reproduced from the Bathymetric Chart of Toyama Bay (Hydrographic Department, Maritime Safety Agency, 1988). Heights are given in meters. The active faults are taken from the bathymetric chart by the Maritime Safety Agency (No. 6334S). The major faults F1 and F2 have something to do with this earthquake event. The northeastern tip of the Noto Peninsula is almost at Suzu City; SUZU in the figure indicates the center of the city.

features around the source region.

Hypocenter Determination

After the 1983 Japan Sea earthquake of M7.7, researchers and government agencies recognized the necessity of intensification of observations in the eastern margin of Japan Sea. From 1985 to 1989, the Earthquake Research Institute, University of Tokyo set up 6 stations on Awashima Island and Sado Island in Niigata Prefecture, Hegurazima Island off northern Noto Peninsula, and the northern end of Noto Peninsula. The Disaster Prevention Research Institute, Kyoto University established 3 stations on the Noto Peninsula and around Toyama Bay (Fig. 1). Table 1 lists the stations (including one previously established).

We selected five stations, HGR on Hegurazima Island, HRJ, NNJ, AHJ on the Noto Peninsula and FKA on Sado Island, as a standard set (S1), which are relatively close to and encircle the source region, to be used for the hypocenter determination. Exclusion of far distant stations avoids the complexity of heterogeneous crustal structure. The involvement of data from other stations, WJM, NUJ and SWD, whose epicentral distances are

Table 1. Seismic stations used. The stations HRJ, NNJ, AHJ are attached to the Disaster Prevention Research Institute, Kyoto University; others to the Earthquake Research Institute, University of Tokyo. Station correction term for P time at NUJ is given.

Code	Location	Longitude (°E)	Latitude (°N)	Altitude (m)	Observation Period	Station Correction (sec)
HRJ	Horyu, Noto Pen.	137.1360	37.3994	275	Dec. 12, 1986–	
NNJ	Nanao, Noto Pen.	136.9649	36.9809	340	Dec. 13, 1985–	
AHJ	Asahi, Toyama	138.5958	36.9233	270	Jun. 1, 1987–	
HGR	Hegurajima Is.	136.9214	37.8485	10	Nov. 25, 1988–	
WJM	Wajima	136.8382	37.3511	360	Nov. 25, 1988–	
FKA	Fukaura, Sado Is.	138.2243	37.8186	160	Jun. 16, 1986–	
SWD	Sawada, Sado Is.	138.2857	38.0520	640	May 22, 1986–	
NUJ	Nou, Niigata	138.0308	37.0478	240	Jun. 2, 1981–	–0.33

comparable to the set S1, has no significant influence on the results, leaving rather large O-C residuals for these stations. The fundamental station set was replaced by another set (S2), i.e., HGR, WJM, NUJ, FKA and SWD during the period from 23:46, February 7, to 23:03, February 8, when stations HRJ, NNJ and AHJ almost missed data due to running out of recording paper. In this case, we used the station correction term for P time at NUJ as listed in Table 1; these were obtained by averaging the O-C residuals calculated in reference to the hypocentral parameters based on the initial standard set of 5 stations. We neglect small absolute residuals less than 0.2s at other stations.

Non-linear equations for hypocentral parameters were solved by minimizing the Basian posterior probability by assuming an *a priori* estimate of the hypocenter (HIRATA and MATSU'URA, 1987). Reading errors in P arrival times are assumed to be 0.1s for the impulsive onset, 0.2s for the emergent and 0.5s for the ambiguous; for S arrivals 0.2s for the impulsive and 0.5s for others.

The structure of seismic wave velocities has not yet been extensively studied in the northern Noto Peninsula region. We have only an explosion seismic profile relatively close to the studied area; from off the western Noto Peninsula to the Atsumi Peninsula, Aichi Prefecture, central Japan (AOKI *et al.*, 1972). This profile shows that the Conrad and Moho discontinuities around the coast of the Japan Sea are at depths of 10–12km and 16–18km, respectively. TSUKUDA (1987) studied the travel times for a subcrustal earthquake with depth of 22km on the coast of western Niigata Prefecture and found strong anisotropy in apparent seismic velocities, which may be due to lateral heterogeneity of the medium, in the Noto and Toyama Bay area. KATO *et al.* (1990) conducted multichannel seismic reflection and refraction experiments in the sea around Sado Island. The refraction survey disclosed a 5.9km/s layer at a depth of about 7km for the profile between off the northeastern tip of the Noto Peninsula and off southern Sado Island. We assume the velocity structure model shown in Fig. 3, roughly consistent with the above information.

We calculated hypocenters for 335 events for the station set S1 and adopted 322 events excluding events with large O-C residuals over 1.0s in P and S arrivals. Among them 180 events have small average residuals: less than 0.2 s for P and 0.6 s for S. The high precision foci are located within the depth range from 10 to 20km; all the events fixed on

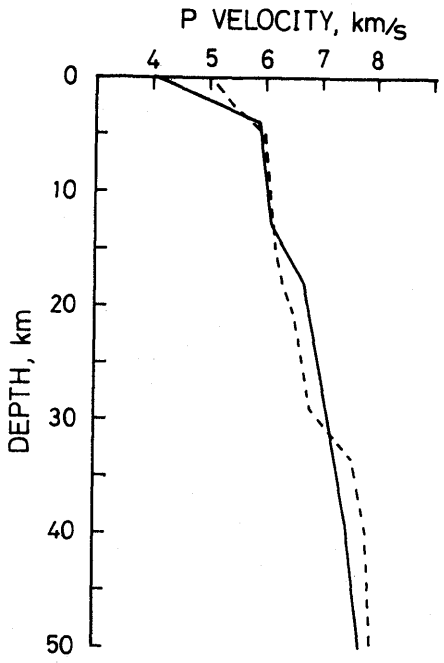

Fig. 3. Velocity structure models. The solid line is for hypocentral determination in the near field; the broken line for focal mechanisms in the far field.

the ground surface are those of low precision. The data set S2 gives 24 foci with the same level of high precision as above. We adopted a total of 346 events for hypocentral distributions studied as follows. Figures 2 and 4 show the distributions of aftershocks. Table 2 is the list of hypocenters with magnitude 3.5 and above.

To confirm degrees of accuracy in hypocenters and the effect of the station configuration on the hypocentral determination, a simulation was conducted: Reading errors are added to P and S times to form disturbed hypocentral data. If we assume the reading errors take ±0.2s for P and ±0.4s for S times, the simulation yields the standard deviations of hypocentral errors 0.9km, 0.7km and 2.0km for the E-W, N-S directions, and depth, respectively, for the mainshock. The extent of the disturbed hypocenters for the mainshock is shown in Fig. 5, together with that for an aftershock which took place in the eastern part of the aftershock area. Most of the actual reading errors are considered to be around ±0.1s and ±0.2s for P and S phases; therefore, the average hypocentral errors are less than half of the above range of the simulated hypocenters.

For an event shallower than about 10km, the accuracy is somewhat decreased so that the focal depth is apt to be beyond the ground surface level, so we fix it at the surface (Fig. 4). Even in this case, the epicenter is somewhat stable to the reading errors, which can be easily recognized from the simulation (Fig. 5).

Depths of most of the foci are confined to the range between 10km and 15km

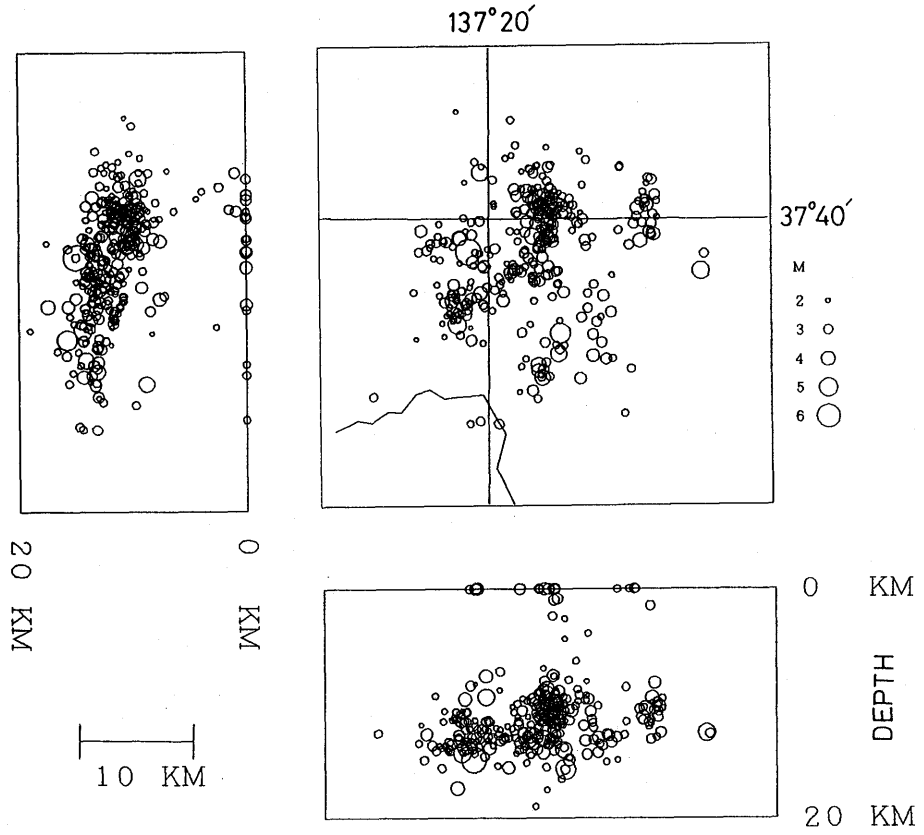

Fig. 4. Hypocentral distribution of aftershocks. The largest shock is the mainshock.

(Fig. 4). These depths are consistent with the later phases observed on the seismograms at some stations as follows.

Station FKA at the southwestern tip of Sado Island often captured a remarkable seismic phase several tens of seconds after the S wave onset on the aftershock seismograms as shown in Fig. 6. Epicentral distances of 77–81km and travel times of about 50–54s yield the apparent velocities for this wave of 1.50–1.57km/s, which correspond to the sound velocity in sea water. This phase is interpreted to be the so called T phase, which is often found on seismic waves which are propagated through the ocean. This phase was first noticed by LINEHAN (1940) and studied observationally by TOLSTOY and EWING (1950), EWING *et al.* (1952) and others. Excitation of T phases means that the source should be located at a shallow depth. The depth should not be much greater than the distance between the source and the conversion point from seismic waves to sound waves, which is estimated within 10–20km considering the apparent velocity and its relatively sharp onset. Events with high T amplitudes greater than S waves were concentrated in the southern aftershock areas, while the events with no T phase took place in the northernmost region. Since the clustered aftershocks show no significant depth change as shown in Fig. 4, the

Table 2. List of hypocenters for shocks with magnitude 3.5 and greater.

Y	M D	H M	S (JST)	Longitude (°E)	Latitude (°N)	Depth (km)	M
1993	2 7	2227	43.67	137.3127	37.6407	14.9	6.6
1993	2 8	0 9	24.68	137.3253	37.6079	7.6	3.9
1993	2 8	013	51.60	137.3920	37.6539	7.6	3.7
1993	2 8	050	8.02	137.3153	37.6033	0.0	3.6
1993	2 8	2 6	6.85	137.3249	37.7028	9.5	4.6
1993	2 8	231	5.47	137.3170	37.6324	0.0	3.7
1993	2 8	611	11.08	137.3862	37.6487	9.0	3.6
1993	2 8	1111	59.25	137.3842	37.6450	0.0	3.7
1993	2 8	1238	57.65	137.3867	37.5418	8.8	4.4
1993	2 8	1910	7.49	137.3037	37.6513	9.6	3.9
1993	2 8	23 3	55.01	137.3862	37.6776	10.1	3.8
1993	2 9	731	31.24	137.2960	37.6018	17.4	4.0
1993	2 9	750	59.42	137.3514	37.8072	10.4	3.5
1993	2 9	913	27.52	137.3720	37.6642	9.7	3.7
1993	2 9	1043	2.10	137.3951	37.6888	9.8	3.7
1993	210	19 1	15.96	137.3909	37.6483	11.7	3.5
1993	210	20 7	41.75	137.2980	37.6059	13.3	3.5
1993	211	2117	6.36	137.3032	37.6516	13.9	4.1
1993	213	326	8.00	137.3769	37.6529	10.0	4.4
1993	213	624	19.59	137.3477	37.6021	15.6	3.7
1993	215	349	33.94	137.3974	37.6486	10.4	3.5
1993	215	2347	55.57	137.3591	37.6268	13.4	3.5
1993	216	151	17.15	137.3013	37.5833	14.3	5.0
1993	216	1116	45.70	137.3935	37.6748	10.9	3.5
1993	217	331	50.69	137.2978	37.6146	12.8	3.5
1993	218	1156	54.39	137.5462	37.6255	12.6	4.8
1993	219	2253	25.00	137.4248	37.5410	13.3	3.5
1993	222	556	56.60	137.4915	37.6776	9.6	4.0
1993	222	1412	18.39	137.2198	37.2814	14.1	4.7
1993	222	2329	47.36	137.3940	37.6516	10.6	3.5
1993	223	416	10.52	137.3932	37.6290	10.8	3.5
1993	223	840	45.70	137.3289	37.6288	13.9	3.7
1993	224	956	16.11	137.4991	37.6546	10.3	3.7
1993	224	2228	22.84	137.4376	37.5592	13.0	3.7
1993	227	052	10.50	137.4940	37.6561	8.2	3.6
1993	227	223	56.21	137.2651	37.6571	12.7	3.6
1993	3 4	13 1	55.58	137.4827	37.6750	11.3	4.0
1993	3 7	15 9	23.60	137.4852	37.6495	10.4	4.1
1993	311	1157	60.01	137.4105	37.6713	10.7	3.8
1993	316	1621	27.70	137.3789	37.6175	9.2	3.5
1993	327	2243	34.39	137.4083	37.6087	14.9	3.5
1993	328	523	61.70	137.3714	37.6883	13.5	3.8
1993	4 1	1213	6.23	137.3960	37.6574	11.5	3.7
1993	4 2	2149	52.65	137.4032	37.5605	14.1	4.5
1993	4 3	12 8	35.20	137.3108	37.5912	13.6	3.5
1993	4 5	435	0.31	137.3831	37.5515	13.1	4.3
1993	4 5	1223	37.91	137.3831	37.5473	14.3	3.9
1993	422	1129	10.38	137.3811	37.6630	10.5	3.6
1993	5 7	457	58.92	137.4048	37.5765	15.7	5.3
1993	5 8	549	10.99	137.3982	37.6732	11.4	3.5

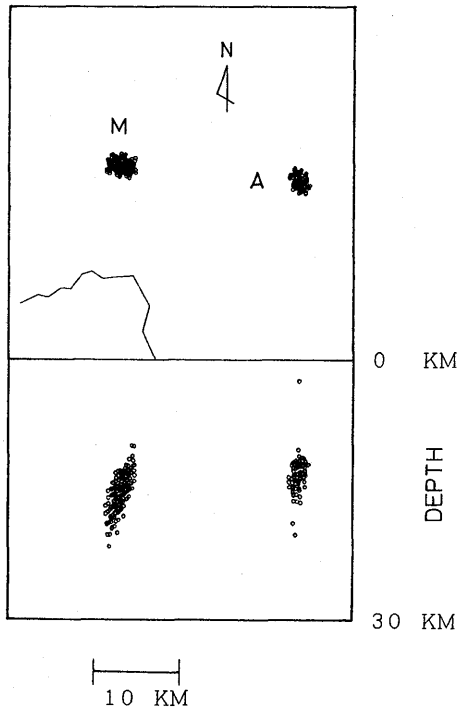

Fig. 5. Simulation of hypocentral errors for the mainshock (M) and an aftershock (A). Reading errors as much as ±0.2s for P time and ±0.4s for S time were added randomly to the reference arrival times. S data were used only for stations HGR and HRJ. This figure shows the simulated hypocentral distribution.

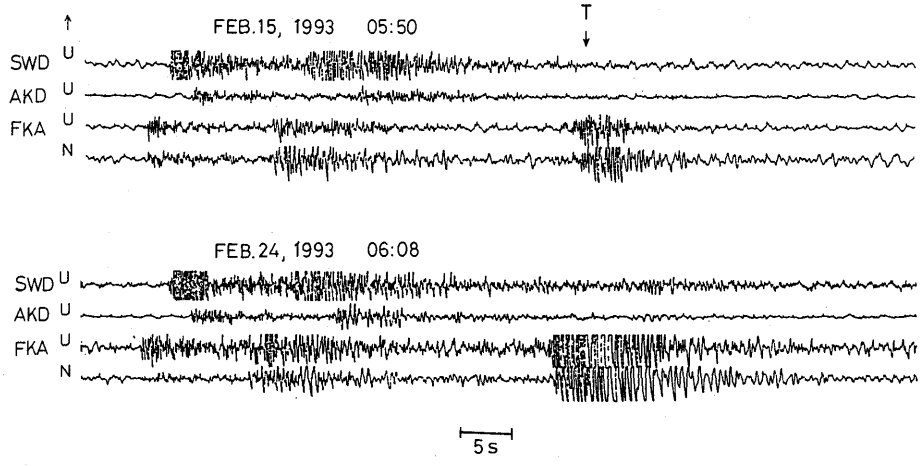

Fig. 6. Seismograms with T phase.

selectivity of emitting T phases may primarily be related to the submarine topography. The deep valley extending eastward off the northeastern tip of Noto Peninsula is considered to be responsible for efficient propagation of sound to station FKA (see Figs. 2 and 13). More detailed analyses and theoretical interpretations will be presented elsewhere.

Another remarkable later phase is found at some stations 2–3s after the P phase, as shown in Fig. 7. This is interpreted as pP or a reflected P wave at the ground surface. The aftershock in Fig. 7 should be located at around a depth of 10km in terms of the travel time analysis.

Aftershock Distribution and Its Tectonic Implications

The source region of the Noto earthquake includes around a sea rise or a small sea ridge striking northeastward from the northeastern tip of Noto Peninsula (Fig. 2). Suzu City, on the northeastern tip of Noto Peninsula, was very close to the source region; eventually the damage was concentrated in this city as described previously. The northwestern side of the ridge is flat and in shallow water. In contrast, there is a steep slope down to Toyama Bay on the southeastern side. Figure 2 shows submarine active faults concentrated on both sides of the sea rise, which were inferred from the sonar survey (KATO *et al.* 1990). A majority of the aftershocks are located around Fault F1 in Fig. 2. Most of the other shocks are associated with Fault F2. These faults lie generally in the N53°E direction.

On the epicentral map, we recognize some predominant clusters of shocks (C1, C2,

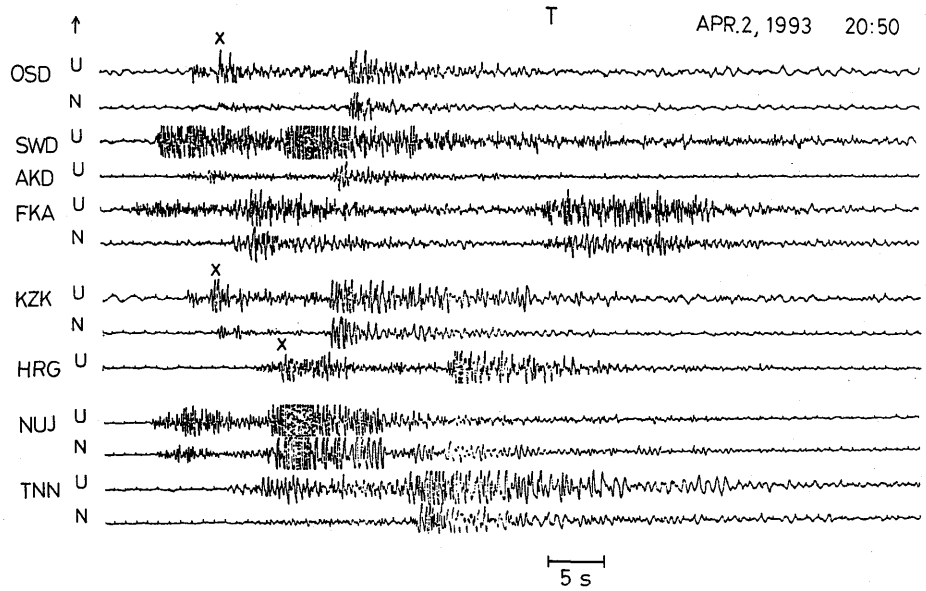

Fig. 7. Seismograms with a remarkable later phase (x) about 2s after the P phase. This phase is interpreted as pP.

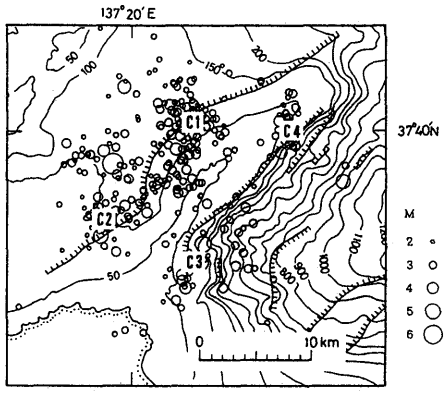

Fig. 8. Clusters of aftershocks. Same as in Fig. 2.

C3, and C4 in Fig. 8). The foci in regions C1 and C4 are aligned in the NS direction. This trend is nearly parallel to the central portion of Fault F1, which is laterally bent in accordance with the irregular trend of extension of the submarine rise.

Figure 9 shows the temporal change of the epicentral distribution. Most of the aftershocks were concentrated in a 15km long narrow zone along Fault F1 during the first 2 days after the mainshock. In the next period from February 10 to 15, the aftershocks were scattered, forming an elliptic high density domain up to 20km in the length of major axis. Simultaneously, activity in the region of Fault F2 started to grow at the southeastern end. The 20km long active zone along Fault F2 has clustered foci at both southwestern (C3) and northeastern (C4) ends, which were predominantly active during the periods from April 1 to May 12, and from February 21 to March 10, respectively. The latter spot gave birth to the largest aftershock on May 7. The maximum extent of the aftershock area is up to 25km in diameter.

In order to estimate the geometry of the fault generated by the mainshock, we take a close look at the structure of the aftershock distribution. Clusters C1 and C2 are considered to occur either on the fault plane of the mainshock or in its vicinity. The predominant clustering spot C1 appeared clearly within a day after the mainshock together with C2. The C1 spot possibly represents the end point of the rupture generated by the mainshock, and existence of a weak zone or a boundary between crustal blocks running nearly north-south. To confirm it we have to study the rupture processes of the mainshock in terms of waveforms from wide frequency band seismograms, which is beyond the scope of this paper.

The clustering aftershocks are not sufficient to delineate the shape of a plane-like fault. We have to resort to relatively large aftershocks, which may partly indicate the place where stresses are highly concentrated due to fault formation by the mainshock. As shown in Fig. 10, there are two northwest dipping planes (FP1 and FP2), which are roughly beneath the surface faults F1 and F2, respectively. The fault due to the mainshock should be FP1. However, the mainshock hypocenter or the initiation point of the rupture is located off the estimated fault plane FP1. The reason for this will be discussed below.

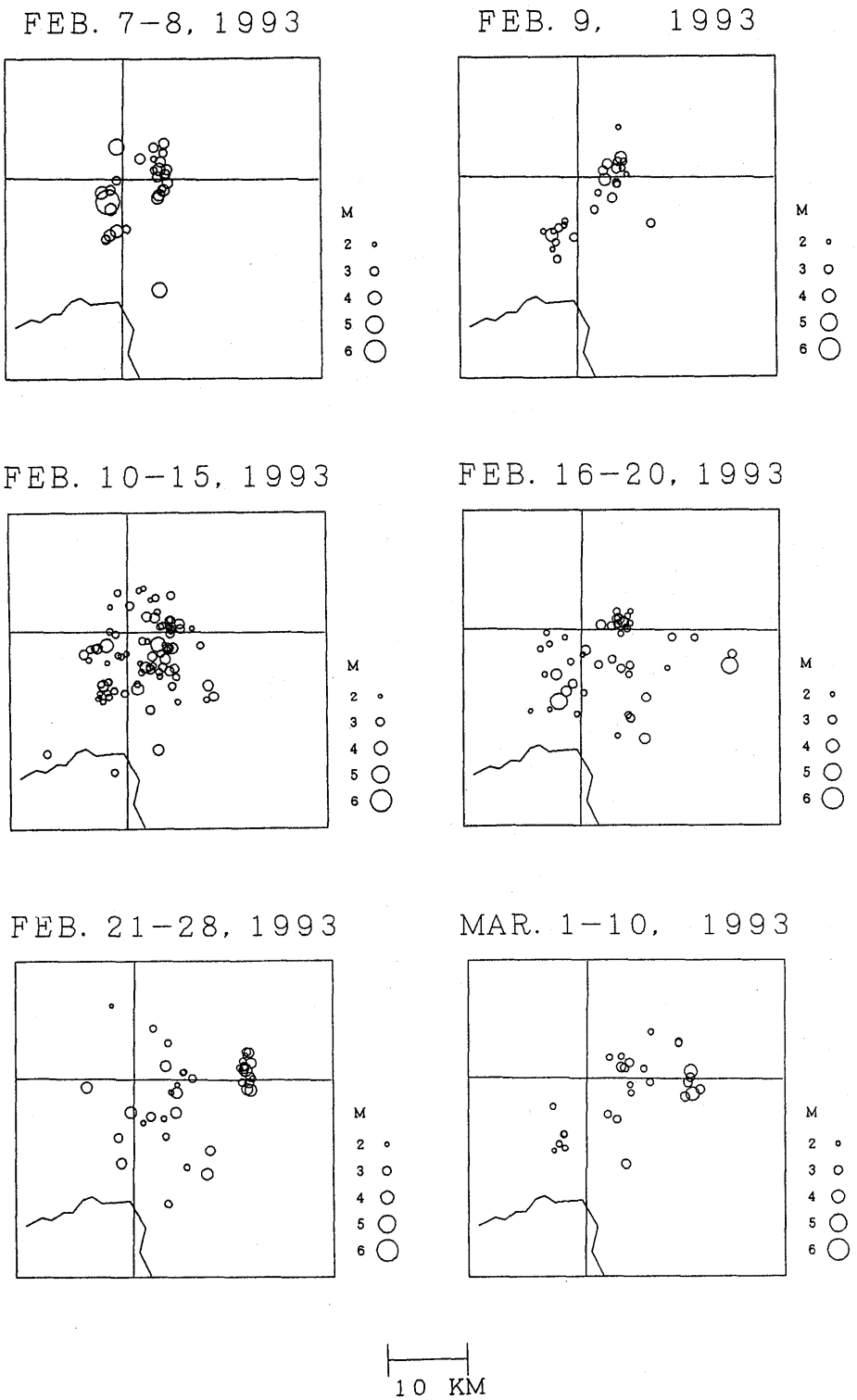

Fig. 9. Epicentral distributions of aftershocks for successive periods.

MAR. 11–20, 1993

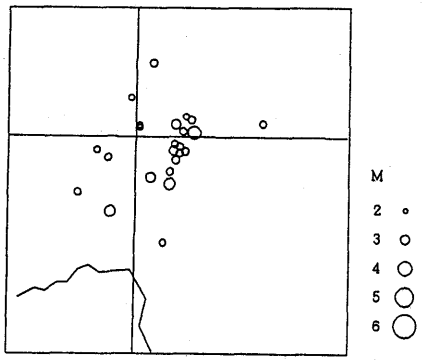

MAR. 21–31, 1993

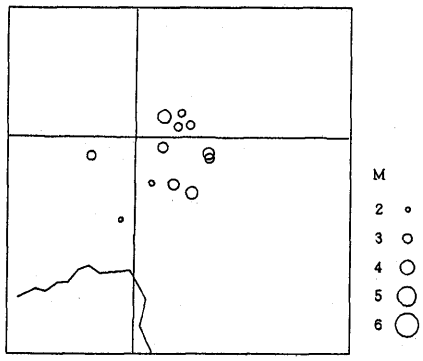

APR. 1–15, 1993

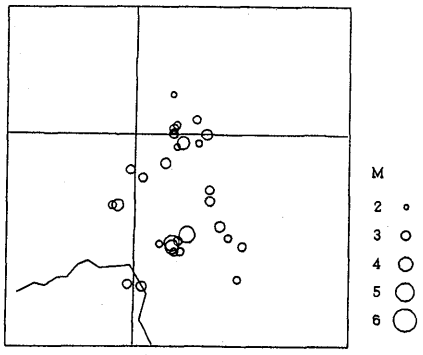

APR. 16–30, 1993

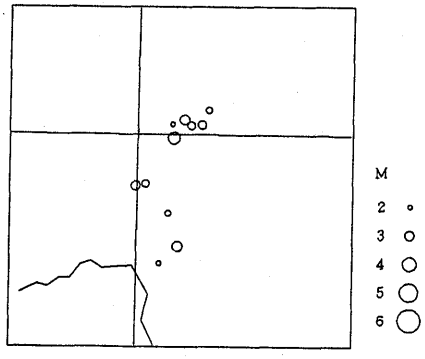

MAY 1–12, 1993

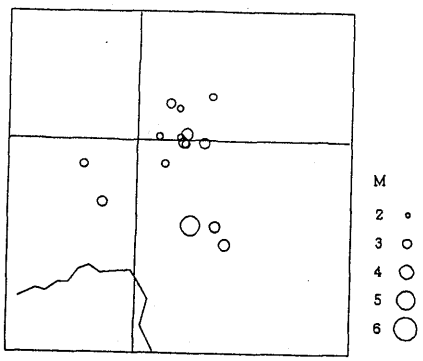

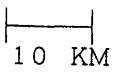

Students of the Earthquake Research Institute, University of Tokyo, have been routinely studying the source mechanisms for large earthquakes (Student Group for Realtime Seismology, 1992). A reverse fault type focal mechanism solution was obtained for the mainshock from the Centroid Moment Tensor (CMT) analysis applied to 9 stations worldwide (Fig. 11). This solution is roughly consistent with the strike direction and dip angle for the estimated fault plane FP1 in Fig. 10. Furthermore, it is in harmony with the solutions previously obtained in the Noto region (e.g. Mikumo and Ishikawa, 1987). Particularly, the October 18, 1985 earthquake with M5.7, which occurred tens of

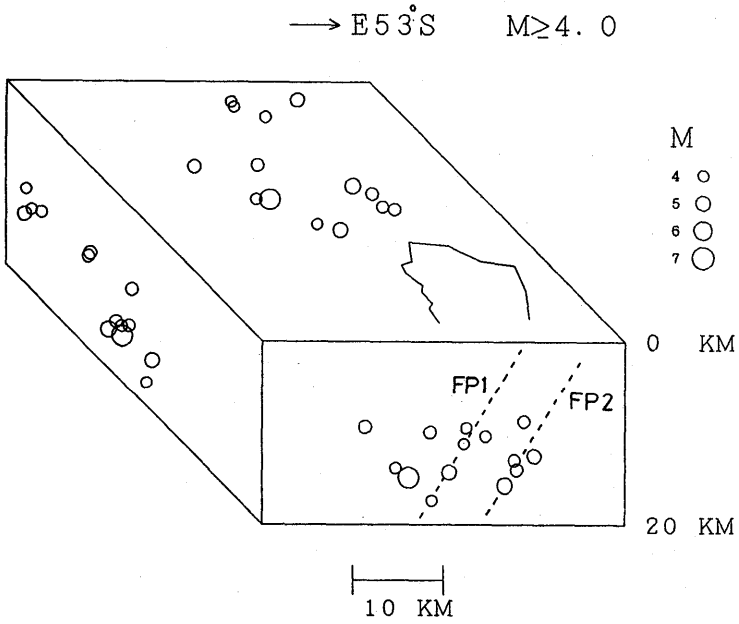

Fig. 10. Hypocentral distribution of major shocks ($M \geq 4$).

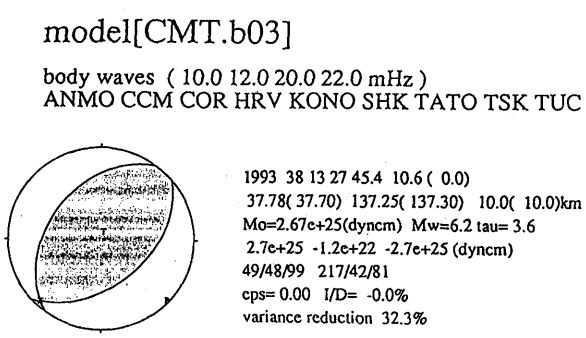

Fig. 11. CMT solution of the mainshock (after Student Group for Realtime Seismology, Earthquake Research Institute, University of Tokyo, 1993; personal communication).

kilometers west of the epicenter of the 1993 event, also has a reverse fault mechanism (DISASTER PREVENTION RESEARCH INSTITUTE, KYOTO UNIVERSITY, 1986).

However, the fault plane solution derived from the initial motions is found to be of a strike slip type rather than a dip slip type with an E-W maximum compressive axis, although there are not a few stations with inconsistent polarity data (Fig. 12). The above two solutions correspond to faulting in the initial and developing stages of rupture, respectively. Moreover, the rupture started at a point not on the fault plane estimated from the large aftershocks. The mainshock consists of at least two events, of which the first is a kind of foreshock. Studies of detailed focal mechanisms for aftershocks to confirm this complex feature of the source process will be presented elsewhere.

It is not certain how the fault planes FP1 and FP2 are related to the surface active faults. First of all, the surface faults are not on the extension of the fault planes FP1 or FP2. Furthermore, the northwest dipping planes and reverse faulting contradict the vertical displacements of faults F1 and F2 shown in Fig. 2. The 1993 Noto earthquake was not the reactivation of the faults that appear on the sea bottom. Nevertheless, the aftershock distribution corresponding to the sea rise topography suggests that the processes for both generating earthquakes and deformation of land and sea bottom surfaces have the same origin.

The Noto Peninsula is well known as a region of dip slip type active faults, in contrast to other regions of southwestern Honshu, Japan, where strike slip events are predominant (OTA *et al.*, 1976). The active fault system extends to the sea bottom around the peninsula. The rise system or the source region of the off Noto Peninsula earthquake is one of them. The SW-NE running fault system associated with the topographic trend of upheaval and subsidence in and around Noto Peninsula is comparable to that of the Shin'etsu region (Niigata and Nagano Prefectures), central Honshu (Fig. 13). The tectonic zone from Noto

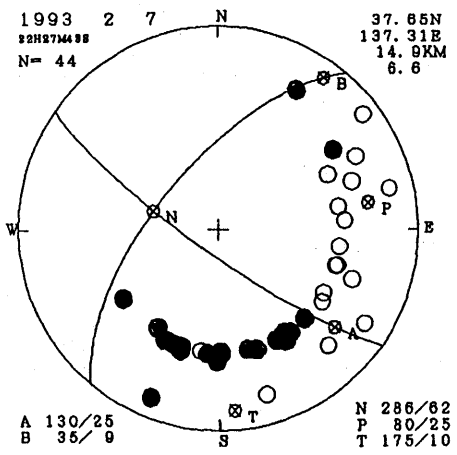

Fig. 12. Focal mechanism of the mainshock, from initial motions (equal area projection on the lower hemisphere). Solid and open circles represent compression and dilatation, respectively.

to Shin'etsu is considered to belong to the large-scale tectonic zone of the eastern margin of the Japan Sea, where NAKAMURA (1983) and KOBAYASHI (1983) proposed a nascent plate boundary between the Pacific and the North American plates.

The Noto earthquake has a widespread aftershock area with some concentrated

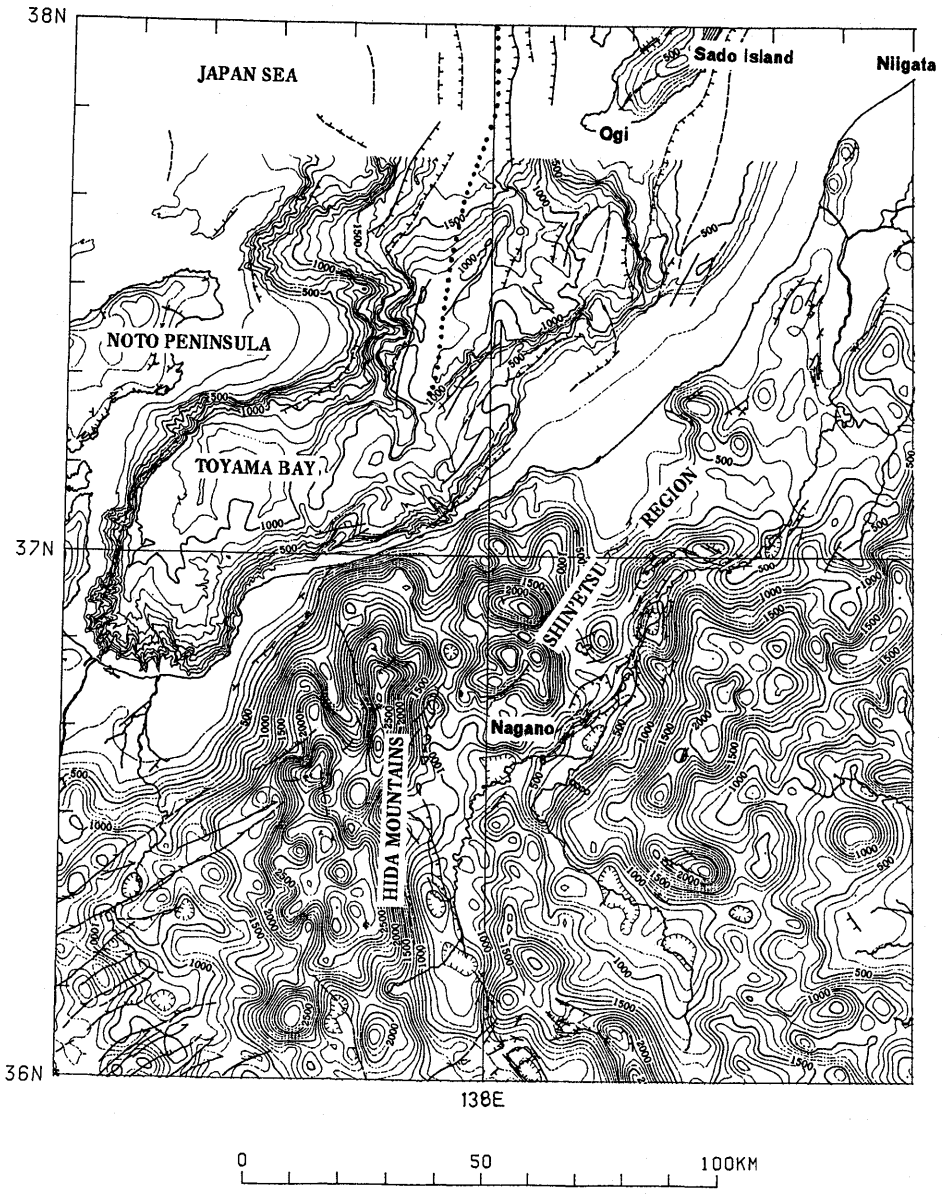

Fig. 13. Tectonic map of the Noto and Shin'etsu regions. Summit level contours on land and submarine topographic contours are given at 100m intervals. Traces of active faults with fluffs indicating the downthrown side are also drawn. This map was originally produced by the Association for the Development of Earthquake Prediction (1989). The large dotted line is the nascent plate boundary proposed by NAKAMURA (1993).

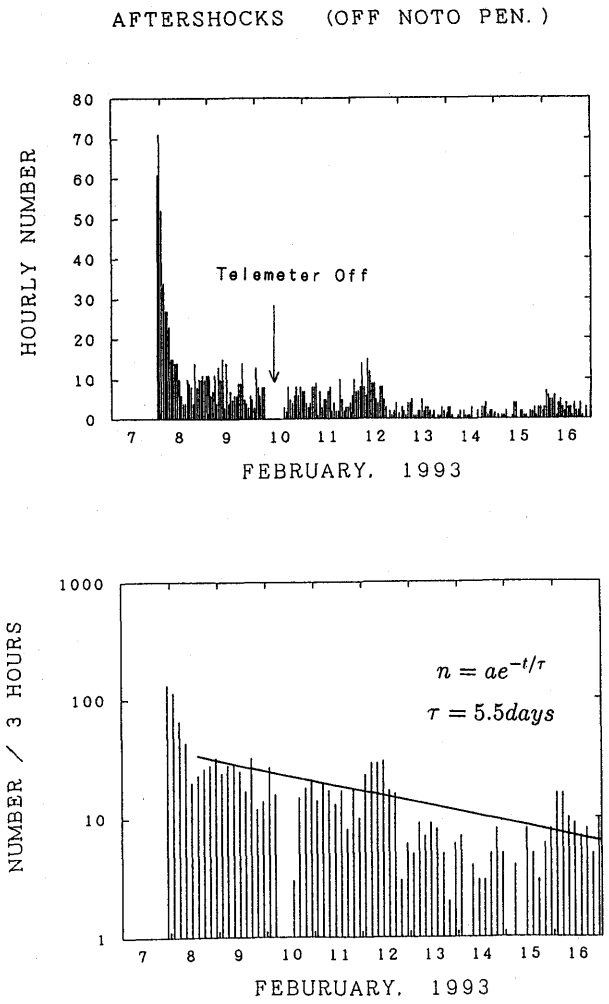

Fig. 14. Time variation of frequency of aftershocks detected at HGR.

activities. This nature may affect the time dependence of aftershocks. The frequency of the aftershocks decays according to the power law $n(t) = at^{-p}$ with p=1.0 during the 10 hours after the mainshock, as similarly as ordinary events. However, the decay curve is roughly represented by an exponential law with time constant of 5.5 days for a long period of more than several days (Fig. 14). As for the Noto earthquake, aftershocks are decaying very slowly or may continue to generate fresh fractures in addition to the ordinary aftershocks.

Conclusions

The hypocenters of the mainshock and aftershocks for the off Noto Peninsula

earthquake of M6.6, which occurred on February 7, 1993, were located using data from telemetered university stations developed in the Japan Sea region. The extent of the aftershock area is up to 25km in diameter. Most of the focal depths are 10–15km, which is consistent with the interpretation of the T phase and pP phase recorded at some stations.

The epicenters of aftershocks are distributed around a sea rise extending in the southwest-northeast direction off the northeastern tip of the Noto Peninsula. The aftershocks during the first two days are well concentrated and aligned on a 15km long narrow zone along one of the major active faults on the northwest side of the rise. Other aftershocks are concentrated in the region along another fault on the southeast side of the rise.

The 3-dimensional structure of the distribution is not clear. The possible fault plane for the mainshock may be the northwestern plane of the two parallel northwestward dipping planes inferred from aftershock hypocenters with magnitude greater than 4. This plane coincides well with one of the fault planes of the CMT solution. The gross structure of the seismic fault is believed to be of the thrust type as in contrast to the strike slip solution obtained from the first motions. The interpretation of this is that the mainshock forms multiple shocks and the first event is of the strike slip type.

The Noto region is included in the tectonic zone along the eastern margin of the Japan Sea, where zonal shortening due to compression is predominant as in the Shin'etsu region, which may be paired with the Noto region in the zone, as revealed by a number of reverse faults taking strikes along the extension of the zone.

Acknowledgments

Dr. Shigeru Kasuga of the Maritime Safety Agency provided us with submarine topographic maps, and staffs at Hokuriku Observatory, Kyoto University, and Takayama Seismological Observatory, Nagoya University informed us of initial motions for focal mechanisms.

References

AOKI, H., T. TADA, Y. SAKATA, I. MURAMATU, H. SHIMAMURA and I. FURUYA, 1972, Crustal structure in the profile across Central Japan as derived from explosion seismic observation, *J. Phys. Earth*, **21**, 197–223.

ASSOCIATION for the DEVELOPMENT of EARTHQUAKE PREDICTION, 1989, A report: Comprehensive studies on seismotectonics, 248pp (in Japanese).

DISASTER PREVENTION RESEARCH INSTITUTE, KYOTO UNIVERSITY, 1986, Seismic activity in the northern Chubu region (including the northern Hida, Toyama Bay and Noto Peninsula regions), *Rep. Coord. Comm. Earthq. Predict.*, **35**, 148–152 (in Japanese).

EWING, M., F. PRESS and J. L. WORZEL, 1952, Further study of the T phase, *Bull. Seism. Soc. Am.*, **42**, 37–51.

HIRATA, N. and M. MATSU'URA, 1987, Maximum-likelihood estimation of hypocenter with origin time eliminated using nonlinear inversion technique, *Phys. Earth Planet. Inter.*, **47**, 50–61.

HYDROGRAPHIC DEPARTMENT, MARITIME SAFTY AGENCY, 1988, Bathymetric Chart of Toyama Bay.

KATO, S., A. ASADA and S. KASUGA, 1990, Tectonic landform and geological structure in the Toyama Trough, southeast margin of Japan Sea, *J. Geography*, **99**, 3–12 (in Japanese with English abstract).

KITAURA, M. (ed.), 1993, Research on the 1993 off Noto Peninsula earthquake, *Research Report of Grant-in Aid for Scientific Research from the Ministry of Education, Science and Culture, Japan*, 77pp (in Japanese).

KOBAYASHI, Y., 1983, On the beginning of subduction, *Earth Monthly*, **5**, 510–518 (in Japanese).

LINEHAN, D., 1940, Earthquakes in the west Indian region, *Trans. Am. Geophys. Union*, **21**, 229–232.
MIKUMO, K. and Y. ISHIKAWA, 1987, Major earthquakes along the eastern to southern margin of the Japan sea and temporal variation of their activity, in relation to regional tectonics, *Proceedings of Earthquake Prediction Research Symposium (1987), National Committee for Seismology, Science Council of Japan and Seismological Society of Japan*, 259–269 (in Japanese with English abstract).
NAKAMURA, K., 1983, Possible nascent trench along the eastern Japan Sea as the convergent boundary between Eurasian and North American plates, *Bull. Earthq. Res. Inst., Univ. Tokyo*, **58**, 711–722 (in Japanese with English abstract).
OTA, Y., T. Matsuda and K. HIRAKAWA, 1975, Active faults in Noto Peninsula, central Japan, *The Quaternary Research*, **15**, 109–128 (in Japanese with English abstract).
STUDENT GROUP for REALTIME SEISMOLOGY, 1992, Realtime determination of mechanisms of recent large earthquakes, *Programme and Abstracts, Seism. Soc. Japan*, 1992 No. 2, 315 (in Japanese).
TOLSTOY, I. and M. EWING, 1950, The T phase of shallow-focus earthquakes, *Bull. Seism. Soc. Am.*, **40**, 25–51.
TSUKUDA, T., 1987, Crustal structure in the northern Fossa Magna and Sado Island regions – A travel time analysis for shocks at around the Moho discontinuity –, *Programme and Abstracts, Seism. Soc. Japan*, 1987 No. 1, 158 (in Japanese).

1993年能登半島沖地震（M6.6）の余震分布とテクトニクスの関係

佃　為成[1)]・和田博夫[2)]・酒井　要[1)]・伊藤　潔[2)]

[1)]東京大学地震研究所
[2)]京都大学防災研究所

1993年2月7日の能登半島沖地震は，禄剛崎沖の南西から北東へ伸びる海底の高まり付近で発生した．この余震の分布をできるだけ精密に求めるため京大防災研上宝観測所と東大地震研信越地震観測所の観測網のデータを統合して震源計算した．この地域の構造はきわめて不均質であり，その影響を極力さけるためもっとも震源域に近い観測点を用いて地震決定を行なった．ほとんどの震源は深さ10～15 km に分布する．佐渡の深浦観測点において大多数の余震についてTフェーズが観測されているが，震源はこのように浅いことを示す．また，いくつかの観測点でpPと解釈できるフェーズが認められる場合があるが，これも震源の深さが10 km 程度であることを支持する．震央は海底の高まりの北西側の活断層に沿って最も密集している．これは本震の地震断層付近の狭義の余震である．広義の余震の主なものはこの海台の南東側の活断層に沿っている．これらの活断層は直接地震断層とは結び付かない．大きな余震分布およびCMT解から推定した地震断層の延長が海底の断層に一致しないからである．しかし，地形や活断層の走向と震央分布の対応のよさは，この地域が活発な変動地域であることを示唆している．初動分布から求めた発震機構は横ずれ型の断層運動を示し，CMT解と一致しない．これは，多重型の地震で，最初の地震が横ずれを起こし，その後逆断層の主断層が生成されたと解釈できる．いずれにせよ能登半島地域は信越地域と同じ日本海東縁に沿った短縮テクトニスク地帯で，そこでは北東－南西走向の逆断層が発達しているが，今回の地震の発生もその短縮運動の一環であろう．